Highly Catalytic Single-Crystal Dendritic Pt Nanostructures Supported on Carbon Nanotubes

Marcos Sanles-Sobrido, Miguel A. Correa-Duarte,* Susana Carregal-Romero, Benito Rodríguez-González, Ramón A. Álvarez-Puebla, Pablo Hervés, and Luis M. Liz-Marzán

Departamento de Química Física, Unidad Asociada CSIC−Universidade de Vigo, 36200, Vigo, Spain

Received December 16, 2008. Revised Manuscript Received February 17, 2009

Herein we describe a one-step method for the preparation of single-crystal, dendritic Pt nanoparticles with no need of organic solvents, templates, or seeded growth. It is shown that Pt nanoparticles with two different shapes—spherical or dendritic—can be efficiently supported onto the sidewalls of carbon nanotubes. Notably, the supported dendritic Pt nanostructrures yield unprecedented catalytic activity, evidenced through the lowest activation energy within an electron-transfer reaction as compared with those reported in the literature for Pt nanostructures.

Catalysis is an essential tool for the development of modern society. More than 95% of the industrial activity, including the fabrication of medical drugs, fuels, or plastics, relies on catalyzed processes in at least one of their stages. Catalysts have as well a key impact on the environment since they are routinely used for the reduction of emissions and have thus become a crucial component in the development of future green technologies, for example, in hydrogen-based fuel cells. Therefore, the big challenge of catalytic activity, selectivity, and design has been brought up, offering a complete breakthrough when related to new, undiscovered properties of nanoparticles and clusters. Indeed, the catalytic activity and selectivity of nanoparticles are strongly dependent on their composition, size, and shape.[1] Platinum is by far the most widely studied catalytic nanomaterial, with an extraordinary projection toward potential catalysis-related applications. However, Pt is expensive and its availability in nature is limited. Thus, a great effort is being devoted to searching for optimized morphologies that would increase the Pt catalytic activity, while decreasing the required amount of material. Pt nanoparticles with several shapes, such as polyhedra,[2−5] nanowires,[6] nanotubes,[7,8] tetrahedra,[9] or dendritic structures,[10−15] have been synthesized by controlled growth on specific crystallographic facets or by templating methods. Mahmoud et al.[16] reported a seeding method, based on the autocatalytic reduction of a Pt complex at the metal surface, for the controlled preparation of uniform, single-crystal Pt nanostars. Interestingly, and in close agreement with Narayanan and El-Sayed,[17] the activation energy for the catalysis of electron-transfer reactions was shown to be shape-dependent. In fact, nanocatalysts that have more atoms on edges or corners (i.e., more valence unsaturated atoms) display a higher catalytic activity, as was found for these star-shaped colloids when compared to other, previously reported, active platinum nanoparticle (NP) shapes.

An additional point that needs to be taken into account is the type of molecules that are adsorbed onto the surface of the nanocatalysts. Unfortunately, amphiphilic polymers or surfactants, necessary for stabilizing high-energy surfaces of the different Pt nanoparticles, reduce the catalytic efficiency of the NPs because they tend to hinder the approach of the reactant molecules to the catalyst surface.[18] Polyvinylpyrrolidone, one of the most widely used templating polymers for shape-controlled NP synthesis, adheres strongly to the nanoparticles surface through a charge-transfer interaction between the pyrrolidone rings and surface Pt atoms,[19] thereby blocking a significant number of active sites. An alternative route for this shape-controlled synthesis relies on altering the reduction

* To whom correspondence should be addressed. E-mail: macorrea@uvigo.es.

(1) Bell, A. T. *Science (Washington, D.C.)* **2003**, *299*, 1688.
(2) Kinge, S.; Bönnemann, H. *Appl. Organomet. Chem.* **2006**, *20*, 784.
(3) Lee, H.; Habas, S. E.; Kweskin, S.; Butcher, D.; Somorjai, G. A.; Yang, P. *Angew. Chem., Int. Ed.* **2006**, *45*, 7824.
(4) Ahmadi, T. S.; Wang, Z. L.; Green, T. C.; Henglein, A.; El-Sayed, M. A. *Science* **1996**, *272*, 1924.
(5) Wang, C.; Daimon, H.; Lee, Y.; Kim, J.; Sun, S. *J. Am. Chem. Soc.* **2007**, *129*, 6974.
(6) Chen, J.; Herricks, T.; Geissler, M.; Xia, Y. *J. Am. Chem. Soc.* **2004**, *126*, 10854.
(7) Kijima, T.; Yoshimura, T.; Uota, M.; Ikeda, T.; Fujikawa, D.; Mouri, S.; Uoyama, S. *Angew. Chem., Int. Ed.* **2004**, *43*, 228.
(8) Mayers, B.; Jiang, X.; Sunderland, D.; Cattle, B.; Xia, Y. *J. Am. Chem. Soc.* **2003**, *125*, 13364.
(9) Tian, N.; Zhou, Z.-Y.; Sun, S.-G.; Ding, Y.; Wang, Z. L. *Science (Washington, D.C.)* **2007**, *316*, 732.
(10) Song, Y.; Yang, Y.; Medforth, C. J.; Pereira, E.; Singh, A. K.; Xu, H.; Jiang, Y.; Brinker, C. J.; vanSwol, F.; Shelnutt, J. A. *J. Am. Chem. Soc.* **2004**, *126*, 635.
(11) Chen, J.; Herricks, T.; Xia, Y. *Angew. Chem., Int. Ed.* **2005**, *44*, 2589.
(12) Teng, X.; Yang, H. *Nano Lett.* **2005**, *5*, 885.
(13) Zhong, X.; Feng, Y.; Lieberwirth, I.; Knoll, W. *Chem. Mater.* **2006**, *18*, 2468.
(14) Teng, X.; Liang, X.; Maksimuk, S.; Yang, H. *Small* **2006**, *2*, 249.
(15) Ullah, M. H.; Chung, W.-S.; Kim, L.; Ha, C.-S. *Small* **2006**, *2*, 870.
(16) Mahmoud, M. A.; Tabor, C. E.; El-Sayed, M. A.; Ding, Y.; Wang, Z. L. *J. Am. Chem. Soc.* **2008**, *130*, 4590.
(17) Narayanan, R.; El-Sayed, M. A. *Nano Lett.* **2004**, *4*, 1343.
(18) Narayanan, R.; El-Sayed, M. A. *J. Phys. Chem. B* **2005**, *109*, 12663.
(19) Borodko, Y.; Habas, S. E.; Koebel, M.; Yang, P.; Frei, H.; Somorjai, G. A. *J. Phys. Chem. B* **2006**, *110*, 23052.
(20) Song, H.; Kim, F.; Connor, S.; Somorjai, G. A.; Yang, P. *J. Phys. Chem. B* **2005**, *109*, 188.

10.1021/cm8033214 CCC: $40.75
Published on Web 03/26/2009

kinetics with foreign ions of metals such as Fe[6,11] or Ag,[20] which allows for the preparation of Pt multipods or nanowires and polyhedra, respectively. Notwithstanding, it is well-known that the catalytic yield of Pt NPs decreases by the presence of these metals at the NP surfaces.[21]

An important role is also played by the nature of the material on which the catalysts are supported. Indeed, the activity of Pt-based catalysts was demonstrated to improve when they are deposited onto carbon supports.[22] Different carbon supports for Pt NP deposition have been reported, including carbon black,[23] carbon nanofibers,[24] ordered activated carbon,[25] and carbon nanotubes (CNTs).[26] CNTs are considered to be ideal candidates due to their remarkable structure-dependent properties,[27−30] including high tensile strength and surface area, together with their high electric and thermal conductivity.[31−33] Moreover, it has been reported that the use of CNTs as supports renders materials that are more resistant against corrosion than for example carbon black,[22,34] permitting as well as better contact between reactant and NP surface than porous carbons (where NPs are trapped within the pores rather than on the outer surfaces).[22,34] Thus, the main reason for the high activity of the Pt/CNT catalyst seems to be that reactant molecules easily arrive at the catalyst and the product molecules readily diffuse away from the Pt particles when supported on CNTs.[35] The enhanced electrocatalytic properties of CNTs are expected, for example, to reduce the amount of precious metal catalyst increasing the commercial viability of proton exchange membrane (PEM) fuel cells.[36,37]

Unfortunately, the efficient attachment of Pt nanoparticles onto CNTs with a uniform distribution remains a challenge because of the high curvature, small size, and chemical inertness of the nanotubes.[38] A common strategy to deposit metal nanoparticles onto CNTs is the functionalization of their external wall by oxidative treatments, with a posterior deposition of the particles.[39−42] However, during this treatment, the one-dimensional electronic structure and the desired properties of the nanotubes may be altered. We have recently developed a method for achieving size- and shape-controlled deposition of NPs without varying the CNT properties, through noncovalent functionalization of the nanotubes combined with polymer wrapping by layer-by-layer techniques.[38,43] When this approach is used, the CNTs surface charge can be controlled preventing damage to their structure and permitting the assembly of charged nanoparticles, such as gold spheres[38] and rods,[44] quantum dots,[45] or magnetic particles.[46,47]

Herein, we report the one-pot synthesis of single-crystal dentritic platinum NPs by means of a combined reduction of K_2PtCl_4 by citrate and borohydride ions. The as-prepared colloids can be successfully assembled onto CNTs, thus rendering a homogeneously loaded hybrid material with clean Pt surfaces, whose catalytic activity was tested on a redox reaction and compared with analogous composites based on platinum nanospheres.

Spherical and dendritic (Pt_s and Pt_d, respectively) NPs of respectively 3 and 20 nm (size defined as the longest distance between two points on a single particle) were successfully synthesized in the presence of citric acid using sodium borohydride as reducing agent. This new and simple approach allows the large-scale preparation of colloids with no need of using nanoparticle seeds or templates. Interestingly, the Pt_d NPs were found to be single crystals, as recently reported for multiarmed Pt nanostructures by Mahmoud et al.[16] but the two-step process was avoided which implies a seed-mediated approach. Additionally, the synthetic approach herein reported does not require the use of undesirable surfactants which could block the active sites on the Pt nanoparticles surface since the obtained Pt nanostructrures are stabilized with a layer of citric acid which shows weak anchoring to the nanocrystals, thus favoring the catalytic activity.

Both negatively charged Pt_s and Pt_d nanoparticles (zeta potential, $\zeta = -20$ mV) were electrostatically assembled onto the (positively) functionalized CNTs.[47] Briefly, the nanotubes were individually functionalized and dispersed in water using polyallylamine hydrochloride (PAH) as a wrapping agent. PAH provides the tips and sidewalls of the nanotubes with

(21) Rioux, R. M.; Song, H.; Grass, M.; Habas, S.; Niesz, K.; Hoefelmeyer, J. D.; Yang, P.; Somorjai, G. A. *Top. Catal.* **2006**, *39*, 167.
(22) Lin, Y.; Cui, X.; Yen, C.; Wai, C. M. *J. Phys. Chem. B* **2005**, *109*, 14410.
(23) Zhou, Z.; Wang, S.; Zhou, W.; Wang, G.; Jiang, L.; Li, W.; Song, S.; Liu, J.; Sun, G.; Xin, Q. *Chem. Commun.* **2003**, 394.
(24) Bessel, C. A.; Laubernds, K.; Rodriguez, N. M.; Baker, R. T. K. *J. Phys. Chem. B* **2001**, *105*, 1115.
(25) Chai, G. S.; Yoon, S. B.; Yu, J. S.; Choi, J. H.; Sung, Y. E. *J. Phys. Chem. B* **2004**, *108*, 7074.
(26) Li, W.; Liang, C.; Qiu, J.; Zhou, W.; Han, H.; Wei, Z.; Sun, G.; Xin, Q. *Carbon* **2002**, *40*, 791.
(27) Wildoer, J. W. G.; Venema, L. C.; Rinzier, A. G.; Smalley, R. E.; Dekker, C. *Nature (London)* **1998**, *391*, 59.
(28) Odom, T. W.; Huang, J.-L.; Kim, P.; Lieber, C. M. *Nature (London)* **1998**, *391*, 62.
(29) O'Connell, M. J.; Bachilo, S. M.; Huffman, C. B.; Moore, V. C.; Strano, M. S.; Haroz, E. H.; Rialon, K. L.; Boul, P. J.; Noon, W. H.; Kittrell, C.; Ma, J.; Hauge, R. H.; Weisman, R. B.; Smalley, R. E. *Science (Washington, D. C.)* **2002**, *297*, 593.
(30) Fujiwara, M.; Oki, E.; Hamada, M.; Tanimoto, Y.; Mukouda, I.; Shimomura, Y. *J. Phys. Chem. A* **2001**, *105*, 4383.
(31) Ebbesen, T. W.; Lezec, H. J.; Hiura, H.; Bennett, J. W.; Ghaemi, H. F.; Thio, T. *Nature* **1996**, *382*, 54.
(32) Baughman, R. H.; Zakhidov, A. A.; de Heer, W. A. *Science (Washington, D.C.)* **2002**, *297*, 787.
(33) Treacy, M. M. J.; Ebbesen, T. W.; Gibson, J. M. *Nature (London)* **1996**, *381*, 678.
(34) Xing, Y. *J. Phys. Chem. B* **2004**, *108*, 19255.
(35) Takashi, O.; Shinji, I.; Inoue, M. *Catal. Commun.* **2007**, *8*, 701.
(36) Kongkanand, A.; Kuwabata, S.; Girishkumar, G.; Kamat, P. *Langmuir* **2006**, *22*, 2392.
(37) Girishkumar, G.; Rettker, M.; Underhile, R.; Binz, D.; Vinodgopal, K.; McGinn, P.; Kamat, P. *Langmuir* **2005**, *21*, 8487.
(38) Correa-Duarte, M. A.; Sobal, N.; Liz-Marzan, L. M.; Giersig, M. *Adv. Mater.* **2004**, *16*, 2179.
(39) Guo, D.-J.; Li, H.-L. *J. Electroanal. Chem.* **2004**, *573*, 197.
(40) Tang, H.; Chen, J. H.; Huang, Z. P.; Wang, D. Z.; Ren, Z. F.; Nie, L. H.; Kuang, Y. F.; Yao, S. Z. *Carbon* **2004**, *42*, 191.
(41) Yu, R.; Chen, L.; Liu, Q.; Lin, J.; Tan, K.-L.; Ng, S. C.; Chan, H. S. O.; Xu, G.-Q.; Hor, T. S. A. *Chem. Mater.* **1998**, *10*, 718.
(42) Li, W.; Liang, C.; Zhou, W.; Qiu, J.; Zhou, Z.; Sun, G.; Xin, Q. *J. Phys. Chem. B* **2003**, *107*, 6292.
(43) Correa-Duarte, M. A.; Liz-Marzan, L. M. *J. Mater. Chem.* **2006**, *16*, 22.
(44) Correa-Duarte, M. A.; Perez-Juste, J.; Sanchez-Iglesias, A.; Giersig, M.; Liz-Marzan, L. M. *Angew. Chem., Int. Ed.* **2005**, *44*, 4375.
(45) Grzelczak, M.; Correa-Duarte, M. A.; Salgueiriño-Maceira, V.; Giersig, M.; Diaz, R.; Liz-Marzán, L. M. *Adv. Mater.* **2006**, *18*, 415.
(46) Correa-Duarte, M. A.; Grzelczak, M.; Salgueirino-Maceira, V.; Giersig, M.; Liz-Marzan, L. M.; Farle, M.; Sierazdki, K.; Diaz, R. *J. Phys. Chem. B* **2005**, *109*, 19060.
(47) Grzelczak, M.; Correa-Duarte, M. A.; Salgueiriño-Maceira, V.; Rodríguez-González, B.; Rivas, J.; Liz-Marzán, L. M. *Angew. Chem., Int. Ed.* **2007**, *46*, 7026.

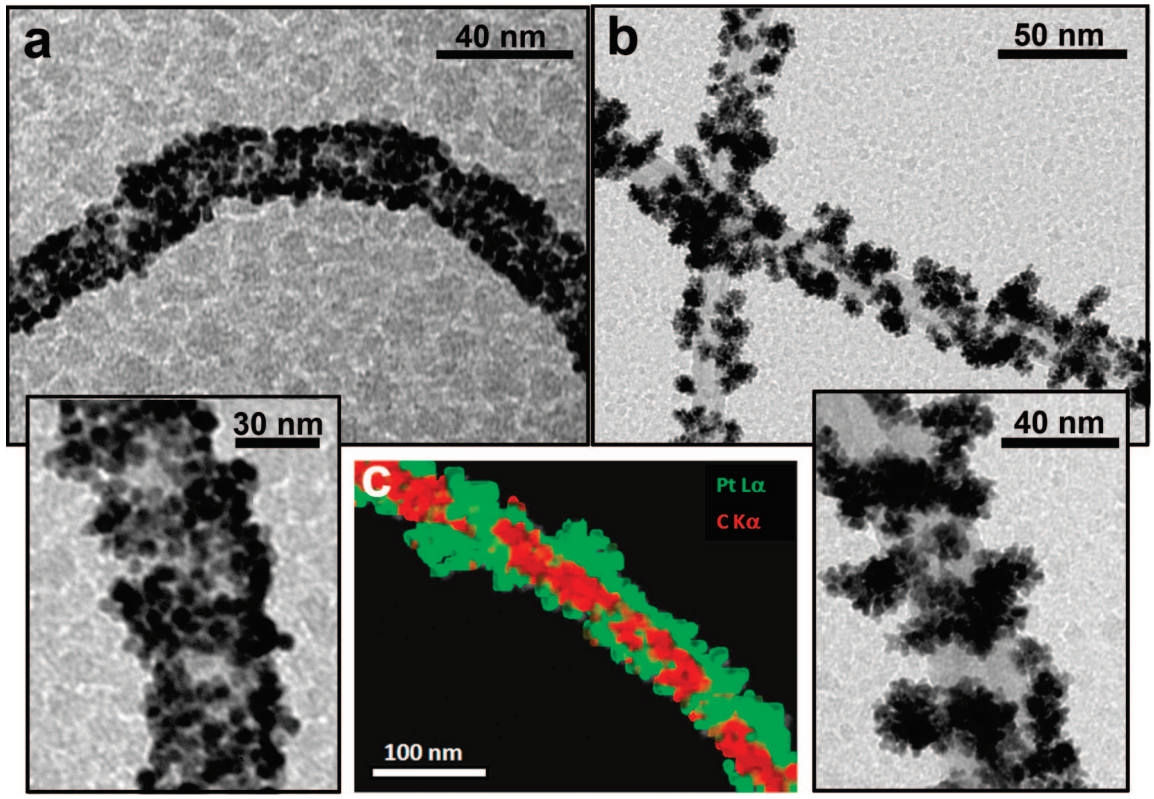

Figure 1. TEM micrographs at two different magnifications, of spherical (a) and dendritic (b) Pt nanoparticles assembled onto the CNTs surface. STEM (c) XEDS elemental mapping of C and Pt for a Pt_d-coated carbon nanotube, demonstrating the core−shell structure of the composite material.

a positively charged surface ($\zeta = +40$ mV), rendering them suitable for the electrostatic adsorption of presynthesized nanoparticles. Importantly, both types of Pt NPs preserve their morphology and are homogenously distributed over the entire nanotube surface (Figure 1).

Pt_s nanoparticles, synthesized by reduction with $NaBH_4$ and stabilized through sodium citrate adsorption, have been widely reported and broadly studied. We carried out a complete characterization of CNT/Pt_d for comparison with CNT/Pt_s, which could be considered a model system. A scanning transmission electron microscopy (STEM) analysis of the samples was performed to evidence the formation of the expected core(CNT)/shell(Pt) structure. STEM-XEDS elemental mapping of the hybrid structures (Figure 1c) showed the relative elemental distribution, with red areas corresponding to the CNT (C K_α line) and green areas corresponding to Pt_d (Pt L_α line). The image clearly shows that the CNTs are located in the inner side while Pt covers the outer part, as expected for the proposed CNT-supported nanoparticle structure.

HRTEM images of the CNT/Pt_d composites (Figure 2a−c) allow us to distinguish the unchanged multiwall structure of the CNTs used as substrates, with an intershell distance of 0.34 nm.[48] The fast Fourier transform of the marked area in Figure 2c shows a spot pattern that can be readily indexed as face-centered cubic (FCC) Pt oriented in a [110] zone axis (ICSD No. 41525), evidencing the single-crystalline structure of the Pt_d NPs. Notably, the SAED analysis on one CNT/Pt_d composite (see Supporting Information) shows the Pt diffraction rings, as well a contribution of the CNT fringes corresponding to the (002) layers.[48]Notably, the SAED analysis shows as well a contribution of the CNT fringes corresponding to the (002) layers.[48] Additionally, the intensity distribution on all diffraction rings in the SAED indicates a nonpreferred orientation of the Pt crystal structure with respect to the nanotube planes, as expected from an electrostatic assembly of the nanoparticles onto the CNTs template. The single-crystal nature of the Pt_d NPs suggests that their formation mechanism does not involve the aggregation of previously formed smaller NPs, which should lead to twin planes and/or other defects. Instead, we speculate about the formation of primary clusters which might act as seeds for further dendritic growth as the Pt(II) salt is reduced. We have observed that this dendritic morphology is determined by the molar ratio between Pt(II) salt, stabilizer, and reducing agent concentrations, with an optimal value of 1:1:0.15 ($K_2PtCl_4/Na_3C_6H_5O_7/ NaBH_4$).

The main advantage of this strategy stems from the highly desired NPs "clean" surface, free from strongly binding stabilizing molecules that would block the Pt active sites. The weak interaction between citrate ions and the Pt surface permits near-complete removal during the synthetic procedure (see Experimental Section), as indicated by the IR spectra (Figure 3). In general, similarly prepared colloids show typical bands for citrate and citric acid (C═O (1715 cm^{-1}), asymmetric and symmetric COO^- (1618 and 1385 cm^{-1}, respectively), C−O (1230 cm^{-1}), C−C stretching (1064 cm^{-1}), and C−H deformation (1130 cm^{-1})).[49] In this case however, once the Pt NPs have been assembled onto

(48) Belin, T.; Epron, F. *Mater. Sci. Eng., B-Solid* **2005**, *119*, 105.

(49) Alvarez-Puebla, R. A.; Garrido, J. J.; Aroca, R. F. *Anal. Chem.* **2004**, *76*, 7118.

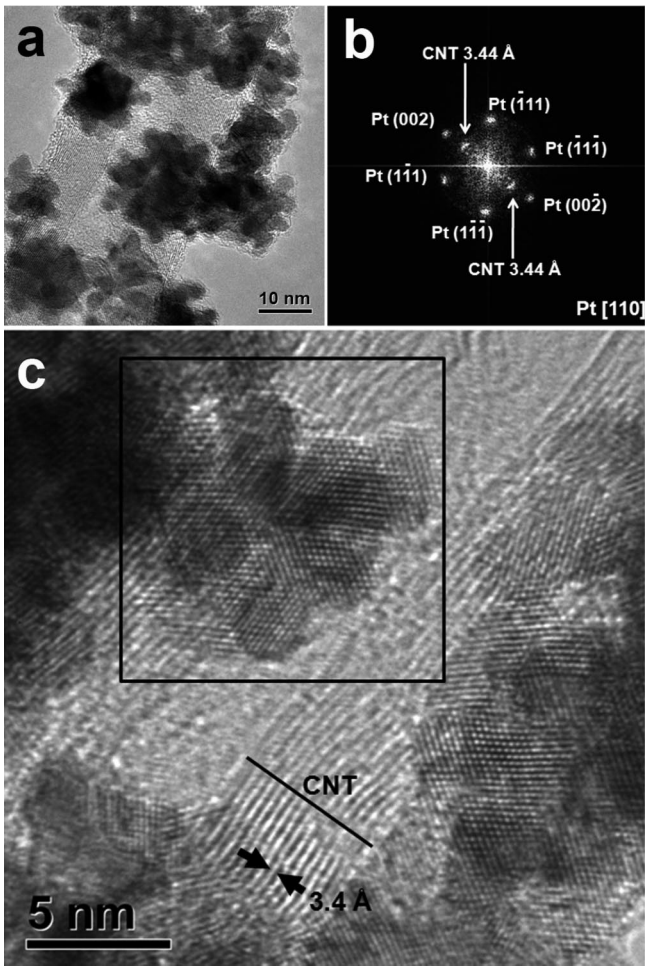

Figure 2. HRTEM (a,c) and SAED analysis (b) of the CNT@Pt_d composite.

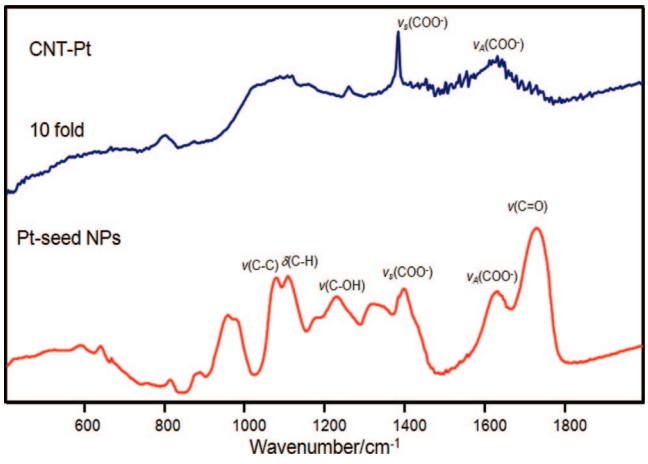

Figure 3. IR spectra of platinum seed colloids compared with that of Pt colloids supported on the CNTs after washing by centrifugation.

the CNTs, the washing cycles (repeated centrifugation and redispersion) practically eliminate all the citrate as shown in the weak bands in the IR spectrum after washing, which mainly include the asymmetric and symmetric COO^- stretchings (at 1616 and 1387 cm^{-1}, respectively).

The catalytic activity of as-prepared CNTs/Pt (with Pt_s or Pt_d NPs) composites was tested using a model reaction where potassium hexacyanoferrate(III) is reduced by $NaBH_4$ into potassium hexacyanoferrate(II).[50] The concentrations of Pt_s

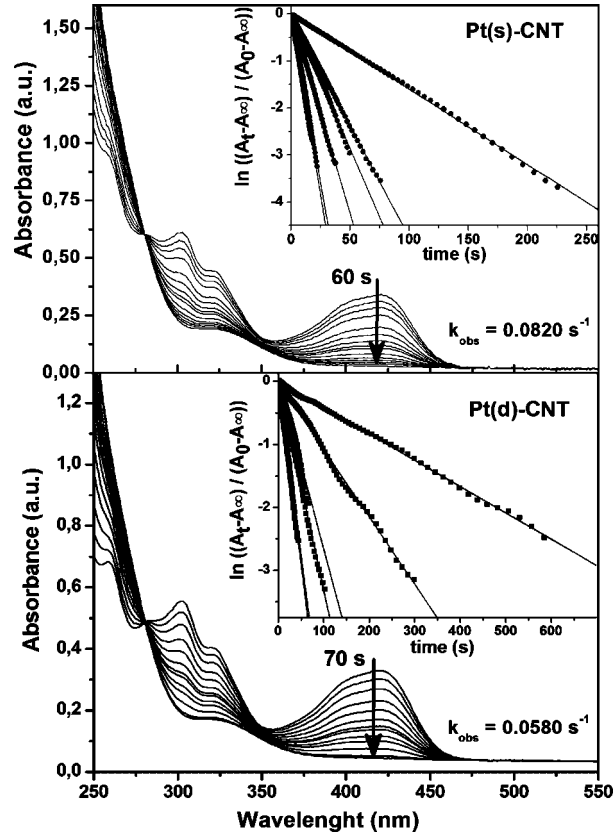

Figure 4. Spectral evolution of hexacyanoferrate in the presence of borohydride and CNT/Pt_s (top) or CNT/Pt_d (down) composites as catalysts. $[K_3Fe(CN)_6] = 5.4 \times 10^{-4}$ M, $[NaBH_4] = 0.011$ M, [Pt(s)-CNT] = 0.40 mg/L, [Pt(d)-CNT] = 2.4 mg/L, pH =13. The insets show the good fit of the experimental results to first-order processes for different catalyst concentrations.

and Pt_d NPs in the composites were similar (41.8 and 43.4 mg mL^{-1}, respectively), as determined by inductively coupled plasma-atomic emission spectrometry (ICP-AES). Since both types of nanostructures were prepared and stabilized in a similar way, we can safely compare the catalytic activity as a function of NP morphology.The catalytic efficiency of both composites was thus tested by monitoring the effect of the CNT/Pt_e and CNT/Pt_d hybrids on the reduction rate of potassium hexacyanoferrate(III) by $NaBH_4$. In all experiments we used $NaBH_4$ concentration in large excess (see Experimental Section) so that, to a good approximation, it can be considered constant throughout the reaction (isolation method); the kinetics of the reduction process can be treated as a pseudo-first-order reaction. The progress of the reduction was monitored through changes in the UV−vis spectra of hexacyanoferrate(III) when using both Pt_s and Pt_d NPs supported onto CNTs (Figures 4a and 4b, respectively). The characteristic hexacyanoferrate(III) absorption band at 420 nm decreases with time as being reduced into ferrocyanide, offering a good correlation with first-order kinetics, as shown in the inset of Figure 4a,b for various catalyst concentrations.

Activation energies (E_a) for the selected reaction were determined by means of an Arrhenius plot,; i.e., the slope

(50) Pastoriza-Santos, I.; Pérez-Juste, J.; Carregal-Romero, S.; Hervés, P.; Liz-Marzán, L. M. *Chem.-Asian J.* **2006**, *1*, 730.

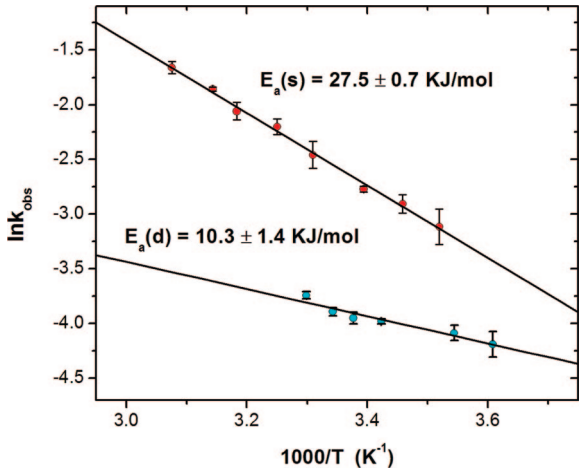

Figure 5. Activation energy (E_a) for the reduction of hexacyanoferrate(III) by sodium borohydride catalyzed by CNTs loaded with spherical nanoparticles E_a(s) and dendritic single crystals E_a(d). Both nanocatalysts are almost free of sodium citrate used as stabilizer.

of the linear relationship between the natural logarithm of the temperature-dependent rate constant and the inverse temperature is $-E_a/R$, where R is the universal gas constant. The value of E_a is used because it is independent of concentration and nanocatalyst surface area. Analysis of the catalytic activity for CNTs loaded with Pt_s and Pt_d revealed a much lower activation energy when the reaction was catalyzed by the dendritic Pt NPs ($E_{a_d} = 10.34$ kJ mol^{-1}, $E_{a_s} = 27.0$ kJ mol^{-1}) (Figure 5), while both values were lower than that reported[51] for the same reaction in the absence of catalyst (31 kJ mol^{-1}). These results are in-line with those reported by Mahmud and co-workers[16] when using multi-armed single-crystal Pt nanoparticles, which offered increased catalytic activity for the reduction of hexacyanoferrate(III) by thiosulfate (from $E_a = 38.3$ kJ mol^{-1} in the absence of catalyst down to $E_a = 14$ kJ mol^{-1}). In the present case, the exceptionally lower E_a determined in the presence of CNT/Pt_d composites can be explained by an increase of Pt atoms at the edges and corners of the multiple arms due to the dendritic shape.

In summary, we have developed a one-step method for the preparation of single-crystal, dendritic Pt nanoparticles with no need of organic solvents, templates, or seeded growth. It was shown that Pt nanoparticles with two different shapes—spherical or dendritic—can be efficiently supported on the sidewalls of CNTs. Additionally, their catalytic activity was studied, and a much lower activation energy was determined for the reduction of hexacyanoferrate(III) by sodium borohydride in the presence of the dendritic CNT/Pt_d heterostructures. This exceptional catalytic behavior can be justified by the presence of many corners and edges in the particles with dendritic shape. Moreover, both the exceptional catalytic properties and synthetic nature exposed for the obtained CNT/Pt hybrid heterostructures make them ideal candidates for the preparation of CNTs composites for PEM fuel cells by means of the layer-by-layer assembly technique.[52]

Experimental Section

CNT Polyelectrolyte Functionalization. CNTs were redispersed in ultrapure water (18 MΩ-cm) as previously described.[38] Briefly, CNTs were dispersed in a 1 wt % aqueous solution of polyallylamine hydrochloride (PAH) up to a concentration of 150 mg/L. A combination of rapid stirring and sonication was used to ensure the presence of well-dispersed, individual nanotubes. Excess PAH was removed by repeated centrifugation and redispersion cycles.

Spherical Platinum Nanoparticles. Spherical Pt nanoparticles were synthesized as follows: to a solution containing 43 mL of ultrapure water, 2.5 mL of sodium citrate (0.1 M) and 2.5 mL of 0.05 M H_2PtCl_6, 2.45 mL of sodium borohydride (0.015 M) was added as reducing agent (citrate/H_2PtCl_4/$NaBH_4$ in a molar ratio of 2:1:0.3). The solution was stirred for 10 min.

Dendritic Platinum Nanoparticles. Dendritic Pt nanoparticles were synthesized as follows: to a solution containing 21.52 mL of ultrapure water, 1.25 mL of sodium citrate (0.1 M) and 1.25 mL (0.1 M) of K_2PtCl_4, 1.22 mL of sodium borohydride (0.0158 M) was added (citrate/K_2PtCl_4/$NaBH_4$ in a molar ratio of 1:1:0.15).

NPs Deposition onto CNTs. CNT@PAH (0.6 mL; 0.5 mg/mL) was added to 50 mL of Pt seeds solution (0.5 mM). After 30 min, the solution was centrifuged (10 min, 8000 rpm) and redispersed in 20 mL of pure water to remove nonadsorbed nanoparticles.

IR Analysis. Selected samples were characterized with transmission FTIR (Bruker, Equinox 55) on pressed KBr pellets (150 mg of KBr and 1 mg of sample). The transmission FTIR cell was flushed with N_2 gas for 10 min before scanning to remove atmospheric water vapor and CO_2 from the spectrophotometer. The spectral resolution was set to 1 cm^{-1} and 32 scans were collected in each spectrum.

ICP-AES Analysis. The sample (dispersion of CNT/Pt_s or CNT/Pt_d) was dried in an oven at 60 °C and calcined for 2 h at 600 °C to remove organic matter. Then, the solid residue was treated with 4 mL of aqua regia (50%) and finally diluted to 25 mL before proceeding with the ICP-OES analysis.

Kinetic Measurements. The reactions were carried out at different temperatures in quartz cuvettes (thermostatted with an accuracy of 0.2 °C), placed in a diode-array UV/vis spectrophotometer (Agilent 8453). All solutions were previously deaerated, and the reaction mixtures were maintained at pH 13 to avoid $NaBH_4$ decomposition.[53] Kinetic data were always satisfactorily fitted by the first-order integrated rate equations in hexacyanoferrate concentration. Experiments were reproducible to within 5%.

Acknowledgment. M.A.C.-D. acknowledges the *Isidro Parga Pondal* Program fellowship (Xunta de Galicia, Spain), and R.A.A-P acknowledges the *Ramón y Cajal* Program fellowship (Ministerio de Educación y Ciencia, Spain). This work has been supported by the Spanish Ministerio de Ciencia e Innovacion (Grants CTQ2007-64758, MAT2008-05755/MAT) and the Xunta de Galicia (Grants PGIDIT06PXIB31479PR, 08TMT008314PR, and 2008/077).

Supporting Information Available: SAED analysis of the CNT/Pt_d composite. This material is available free of charge via the Internet at http://pubs.acs.org.

CM8033214

(51) Freund, T. *J. Inorg. Nucl. Chem* **1959**, *9*, 246.
(52) Michel, M.; Taylor, A.; Sekol, R.; Podsiadlo, P.; Ho, P.; Kotov, N.; Thompson, L. *Adv. Mater.* **2007**, *19*, 3859.
(53) Rheenen, P. R. v.; McKelvy, M. J.; Glausinger, W. S. *J. Solid State Chem.* **1987**, *67*, 151.